

Origin of waters observed along 137°E

Frederick M. Bingham

Center for Marine Science, University of North Carolina at Wilmington, Wilmington, North Carolina, USA

Toshio Suga and Kimio Hanawa

Department of Geophysics, Graduate School of Science, Tohoku University, Sendai, Japan

Received 20 November 2000; revised 16 October 2001; accepted 25 October 2001; published 16 July 2002.

[1] Using the World Ocean Atlas data set, we examine the origins and flow paths of subducted waters observed along the 137°E section in the western North Pacific. The waters studied consist mainly of the water mass known as North Pacific Tropical Water, but includes much of the water midlatitude thermocline. A method is developed to trace these waters from 137°E back through the subtropical gyre to their outcrops. Subducted waters are aged using this technique and found to be between 0.5 and 35 years old by the time they reach 137°E. For this subducted regime, waters on a given isopycnal observed along 137°E increase in age with decreasing latitude, with waters at the southern end of the section being 2–3 times older than waters at the northern end. This estimate of age is consistent with previous estimates calculated from chlorofluorocarbon measurements. It is found that subducted water masses are strongly homogenized by the time they reach 137°E. That is, the originally subducted waters have a wide variation in θ - S characteristics, but by the time they reach 137°E, they form a coherent water mass with a tight θ - S relation. It is shown that isopycnal mixing is not a plausible mechanism for this homogenization but that diapycnal mixing is a more likely process. *INDEX TERMS*: 4283

Oceanography: General: Water masses; 4532 Oceanography: Physical: General circulation; 4572

Oceanography: Physical: Upper ocean processes; 4215 Oceanography: General: Climate and interannual variability (3309); *KEYWORDS*: salinity, hydrography, ocean circulation, Pacific Ocean, northern, water masses, variability

1. Introduction

[2] Time series hydrographic observations in the ocean are valuable pieces of information in assessing interannual and interdecadal variability. An important and interesting time series is the set of observations taken along 137°E in the western Pacific (Figure 1). Other long-term ocean time series have focused on measurements at a single station like the Hawaii Ocean Time series [Karl and Lukas, 1996] or the Bermuda Atlantic Time Series [Michaels and Knap, 1996] programs or ocean weather stations such as Station P [Tabata and Weichselbaumer, 1992] or Station C [Levitus *et al.*, 1994a] or on shallow, upper ocean expendable temperature and salinity measurements, like the long volunteer observing ship expendable bathythermograph (XBT)/expendable conductivity-temperature-depth lines that cross ocean basins [e.g., Roemmich and Cornuelle, 1992; Sprintall *et al.*, 1997; Roemmich *et al.*, 1997]. In contrast, the 137°E section cuts across the entire western Pacific, measuring shallow, intermediate, and deep waters from tropical and subtropical regions (Figure 1). It has been doing so for almost 35 years, constituting a unique record of long-term variability in the gyre-scale structure of the western North Pacific. Other such time series exist [e.g.,

Kessler, 1999], but none have been operating for as long or as consistently.

[3] Although the usefulness of the 137°E data in detecting the oceanic variability along this meridian is quite apparent, it is not always clear what that variability implies for changes in the basin-scale circulation and water mass distribution, the atmospheric forcing, etc. In order to interpret the variability observed along 137°E appropriately in the context of climate change, we need sufficient knowledge about the origin and/or formation history of water in each portion of the section and some idea of what happens to the water between subduction and observation.

[4] One of the most important waters found along 137°E is the North Pacific Tropical Water (NPTW) [Tsuchiya, 1968]. It is characterized as a subsurface salinity maximum in the North Equatorial Current and derived from the high surface salinity area of the central subtropical North Pacific [Suga *et al.*, 2000]. NPTW is formed by the process of midlatitude subduction, which has drawn much recent interest both observational [Joyce *et al.*, 1998] and theoretical [Huang and Qiu, 1994; Qiu and Huang, 1995; Williams *et al.*, 1995]. In subduction, surface water takes part in a convergent wind-driven Ekman flow and flows through the base of the mixed layer [Marshall *et al.*, 1993]. The physics of subduction are complex. They were first described by Stommel [1979], who realized that only water that is present

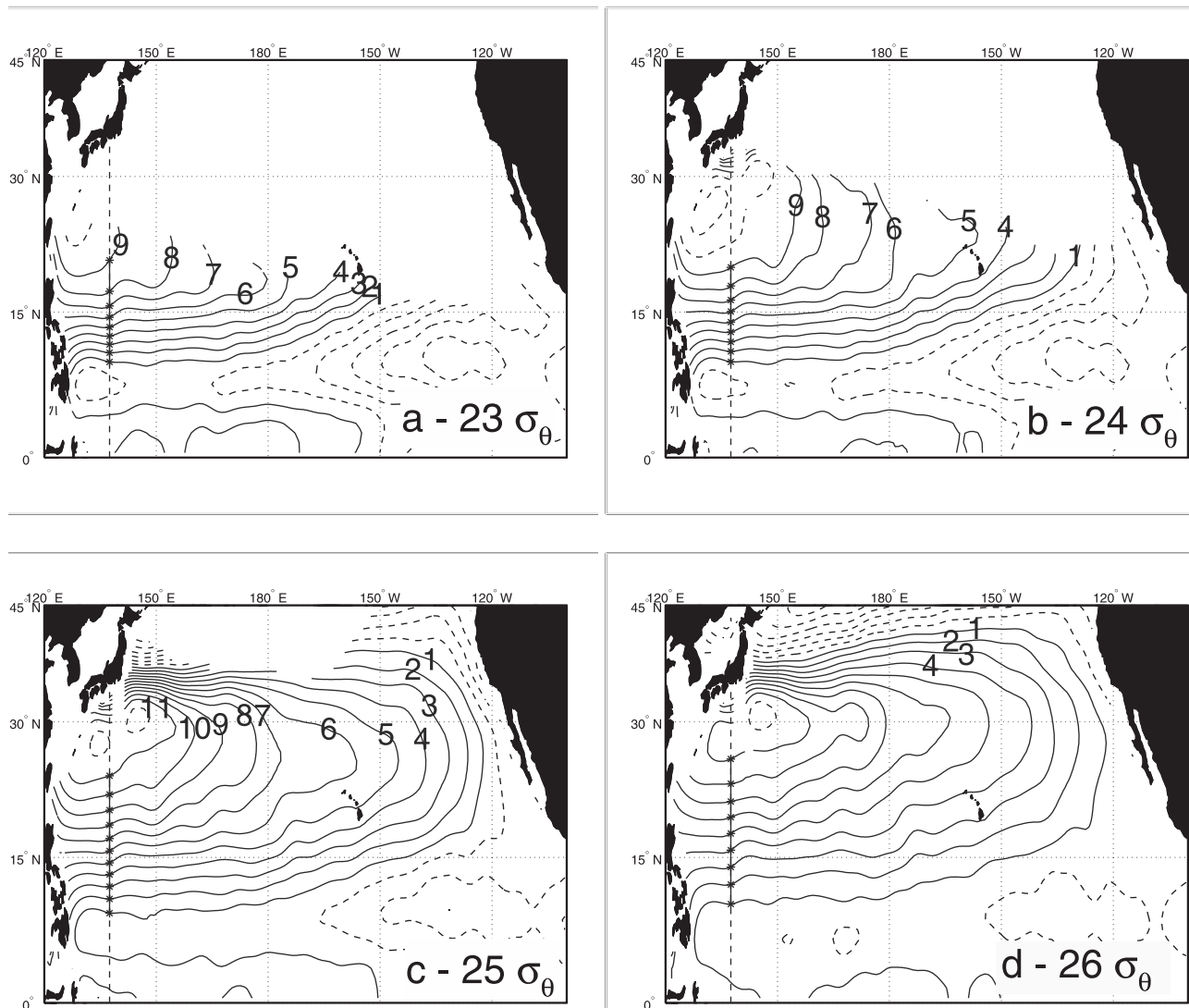


Figure 1. Acceleration potential ($\text{m}^2 \text{s}^{-2}$) on isopycnals: (a) 23.0, (b) 24.0, (c) 25.0, and (d) 26.0 σ_θ . The contour interval is $0.5 \text{ m}^2 \text{ s}^{-2}$. Each map shows the 137°E meridian. The asterisks along 137°E are where the individual streamlines intersect that longitude. Numbers on streamlines are where the outcrop is located according to the reverse trajectory analysis described in the text. Missing numbers in sequence are streamlines where the outcrop could not be determined. Dashed contours are isolines of acceleration potential that were not used in the reverse trajectory analysis calculation.

in the mixed layer in the late winter can subduct into the interior circulation. Subsequent studies [Woods, 1985; Cushman-Roisin, 1987; Marshall *et al.*, 1993] have confirmed this idea and further elucidated the physical processes taking place during subduction. Subduction consists of two parts: vertical pumping through the base of the mixed layer and lateral induction, water flowing geostrophically through a sloping mixed layer base [Qiu and Huang, 1995].

[5] The temporal variability of the water masses observed along 137°E has been addressed by several authors. Suga and Hanawa [1995] showed that interannual variability of North Pacific Subtropical Mode Water (NPSTMW) along 137°E is significantly correlated with the intensity of wintertime cold air outbreaks, which control wintertime

cooling of the surface and ultimately the formation rate and characteristics of NPSTMW. This is an example of how changes in water masses are related to changes in their formation processes associated with ocean-atmosphere interaction.

[6] Shuto [1996] examined interannual variations in the amount of North Pacific Tropical Saline Water (his terminology) or NPTW (our terminology) observed along 137°E . Extreme values in the amount of NPTW observed were shown to be related to extrema in the wind stress curl southeast of Japan with time lags of 0–2 years. This means that when a minimum (maximum) occurs in the wind stress curl, sometime later, an anomalously small (large) amount of a water mass is observed at 137°E . This is consistent with simple subduction theory. A large negative wind stress curl

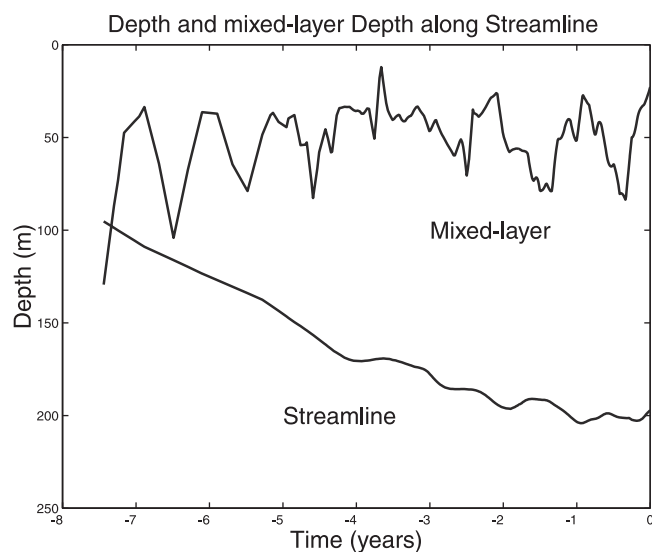


Figure 2. Example of reverse trajectory analysis for streamline 4 on the $25.0 \sigma_{\theta}$ surface (see Figure 1c). The top curve is the mixed layer depth along the path of the streamline. The bottom curve is the streamline depth. The outcrop is where the two curves meet. The abscissa is the time before arrival at 137°E .

induces large vertical pumping at the base of the Ekman layer and results in a large amount of a particular water mass being subducted into the subtropical circulation. That anomalously large amount of water shows up at a later time at a location downstream in the middle of the subtropical gyre. Thus long timescale changes in surface wind-forcing can be observed downstream from where water is subducted as changes in the amount of water observed. What is much less clear is whether interannual variability in the surface characteristics, the potential vorticity, salinity, oxygen, and tracer and nutrient concentrations, of the subducted waters are observable downstream.

[7] Suga *et al.* [2000] also studied the variability of NPTW ($24.0 \sigma_{\theta}$) along the 137°E section. They show changes in the structure and properties of NPTW arriving at 137°E associated with the climate regime shifts in the mid-1970s [e.g., Tanimoto *et al.*, 1993; Yasuda and Hanawa, 1997; Deser *et al.*, 1996]. The NPTW north of 15°N increases in salinity and thickness, while the NPTW south of 15°N increases only in salinity, with the thickness unchanged. They relate these changes to variability in thermohaline forcing and Ekman pumping in the subtropical gyre during the 1970s. They conclude that the salinification of NPTW in the northern part of the 137°E section is a result of an increased volume of formation and transport of NPTW rather than changes in the sea surface salinity, indicating the importance of mixing processes in determining NPTW characteristics at 137°E well downstream of the formation area.

[8] The last example shows that appropriate interpretation of water mass variability observed in the 137°E section requires not only the knowledge about its formation region but also its flow path to the section and possible effects of mixing along the path. As the first step toward under-

standing of these rather complicated processes, we perform a reverse trajectory analysis within the framework of the *World Ocean Atlas 1994 (WOA94)*, where the directly subducted waters at 137°E are traced back to their origin, and examine along-path changes in water mass characteristics.

2. Data Processing

[9] The data used in this study are taken from the *WOA94* [Boyer and Levitus, 1994]. *WOA94* is an analysis of oceanographic data collected in the archives of the U.S. National Oceanographic Data Center that includes monthly averages of temperature and salinity at standard depths in 1° squares. The techniques used to create the objectively analyzed values of temperature and salinity are described in by Levitus and Boyer [1994] and Levitus *et al.* [1994b]. The spatial smoothing employed in producing the *WOA94* averages is over several hundred kilometers.

[10] More up-to-date and possibly more appropriate climatologies for the ensuing calculation have become available recently [Macdonald *et al.*, 2001; Levitus *et al.*, 1998]. The Macdonald *et al.* climatology is as yet untested, but further research may show it to be useful for the type of calculation we will do here. *World Ocean Atlas 1998* is similar to the 1994 version in the North Pacific [Conkright *et al.*, 1999]. The advantages and shortcomings of *WOA94* are well understood. The advantages include: the ease of using a climatology instead of individual casts, and the fact that a climatology gives some indication of average conditions, i.e., eddies are averaged out. The main disadvantage specific to the *WOA94* is that its use is problematic near western boundary currents or fronts [Macdonald *et al.*, 2001]. *WOA94*, or an earlier version [Levitus, 1982], has been used in many ocean general circulation models as a standard observed ocean or initial condition [e.g., Semtner and Chervin, 1988; Hurlburt and Metzger, 1998]. *WOA94* is heavily smoothed, but it remains appropriate for studying interior flows.

[11] The spatial scale used in estimating lateral and vertical gradients throughout this paper is the same as the climatology, 1° in the horizontal, and whatever the standard depth spacing is in the vertical. No further smoothing was done in order to calculate gradients of any quantity.

[12] Maps of acceleration potential [Montgomery and Stroup, 1962; Reid, 1965] relative to 2000 m were prepared for a number of isopycnals between 23.0 and $26.5 \sigma_{\theta}$ using the annual average *WOA94* data (Figures 1a–1d). The 2000 m reference was chosen because it is not so deep as to be near the bottom over most of the North Pacific so it could be applied uniformly. Any chosen reference beneath most of the surface wind-driven flow (1500–2000 m) would give similar results, as deep flows in the North Pacific are generally weak. Examination of the inverse calculation results of Roemmich and McCallister [1989] indicates that 2000 m is a reasonable choice for a uniform reference level.

[13] In maps of acceleration potential on a number of isopycnals in the North Pacific (Figure 1), streamlines end in the north when the annual average surface density becomes greater than the isopycnal being shown. For each isopycnal, one can see the flow of the subtropical

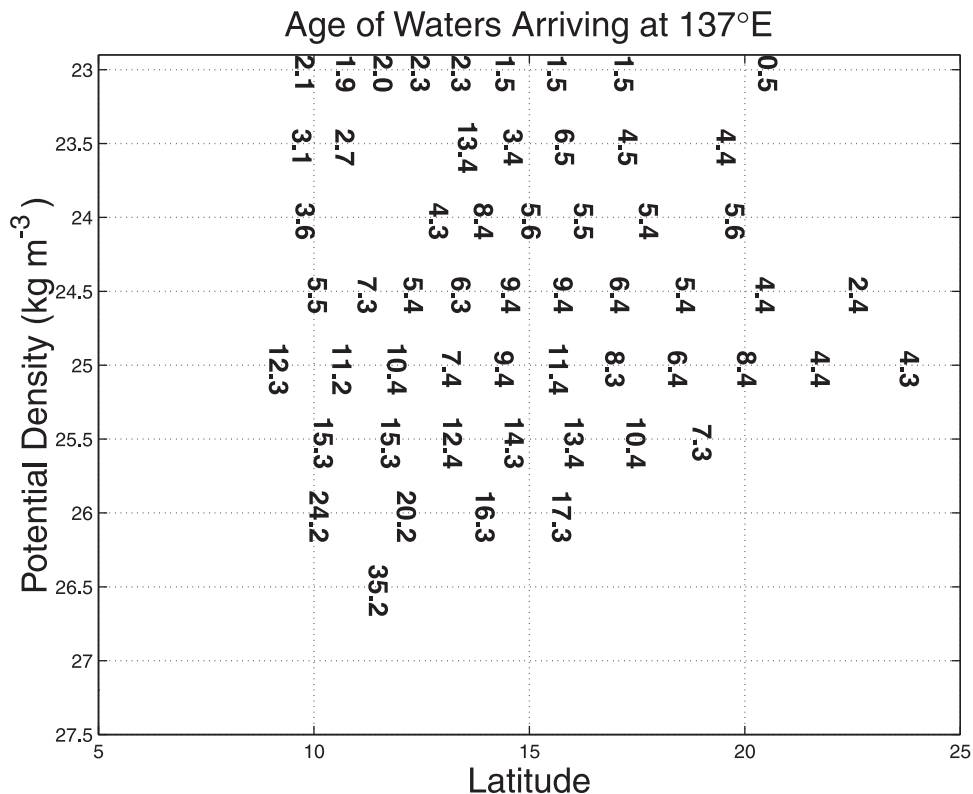


Figure 3. Age in years of streamlines that arrive at 137°E in latitude- σ_θ space. Age is calculated from reverse trajectory analysis by calculating the amount of time to travel along a streamline from outcrop to 137°E.

gyre. For shallow isopycnals like 23.0 and 24.0 σ_θ (Figures 1a and 1b), one only sees the southern half of the subtropical gyre, as the isopycnals outcrop in the middle of the gyre. As one goes deeper, one can see the whole gyre (Figure 1c), including the recirculating part in the northwest. The Kuroshio is represented as a grouping of streamlines in the northwestern part of the gyre. This representation of the Kuroshio is not very realistic (compare with Mizuno and White [1983]) and shows the limitations of the averaging scheme used in producing WOA94. Because of this averaging problem, one must be cautious in interpreting WOA94 data in the vicinity of the Kuroshio, north of 30°N.

3. Reverse Trajectory Analysis

[14] To elucidate the process of subduction and water mass modification along streamlines, a reverse trajectory analysis was applied to some of the streamlines on each isopycnal. For a given isopycnal surface several streamlines that cross the 137°E meridian were chosen. The intersection of each of these streamlines with 137°E is indicated with an asterisk in Figures 1a–1d. We worked backwards along each streamline until it reached the base of the mixed layer. The trajectories were calculated in the following way: Using the maps of acceleration potential, discrete points along the streamlines were located. The intervals between points were variable, with more points where the streamline paths were curved. Starting from

137°E, we took the distance between adjacent points along each streamline and divided by the speed calculated from the flow field. This gave us a time interval between points, which was variable as well. Time intervals were typically 5–10 days; distance intervals were 25–30 km. We moved backward along each streamline from one point to the previous one until the outcrop was reached. Starting dates were arbitrarily taken to be 1 July. Outcrop locations depended a little (on the order of tens of kilometers) on starting date, but not significantly.

[15] WOA94 does include seasonal and monthly averages of temperature and salinity, from which seasonal or monthly streamlines could be calculated. We chose not to do this as the underlying data set is not sufficient to resolve the seasonal variability of the interior circulation. There are probably sufficient data to discern a seasonal cycle of the circulation near the western and eastern boundaries of the North Pacific but not in mid-ocean. In addition, including seasonal variability in streamlines would have made the reverse trajectory calculation extremely complicated and cumbersome, with a lot of additional interpolation in time and space. The basic seasonal cycle of the mixed layer in mid-ocean can be resolved adequately as the signal is larger than in the interior.

[16] Monthly mixed layer depths were calculated from WOA94 data. The mixed layer depth was defined as the depth where the density reaches 0.125 kg m⁻³ greater than the surface value [Huang and Qiu, 1994]. The point where the base of the mixed layer was reached was taken to be

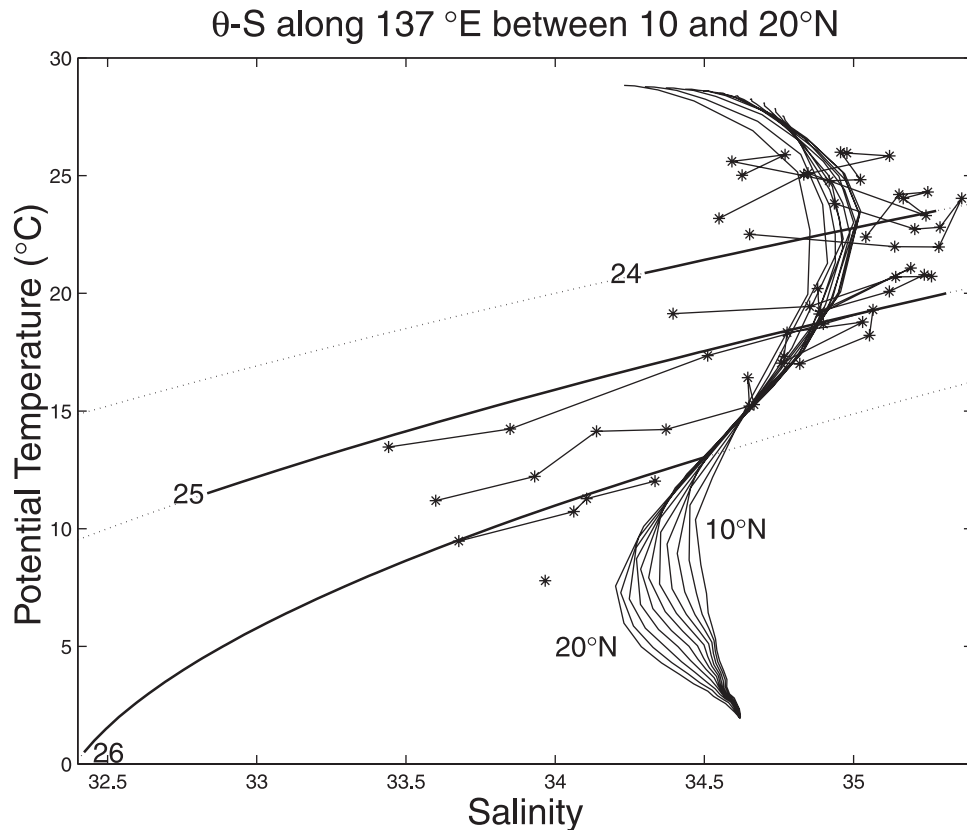


Figure 4. The θ - S relation at isopycnal outcrops (asterisks connected by lines) and averages along 137°E from *WOA94* (lines). The range of curves for 20°–10°N is indicated. Thick lines that cut across horizontally indicate the range of θ and S values along the outcrop of a particular isopycnal in March. Dotted lines continuing the thick lines are the θ - S relation for the given isopycnal. The σ_θ value of the isopycnal is shown by numbers at the end of the thick lines.

the outcrop or the origin of the water mass (numbers in Figures 1a–1d), and the amount of time taken from outcrop to 137°E is defined as the age. Streamlines in Figures 1a–1d with no numerical label did not outcrop in the North Pacific, or the outcrop could not be located using this method.

[17] As an example of the way this method was used, we highlight the analysis for one streamline along the 25.0 σ_θ surface (Figures 1c and 2). One can see the mixed layer getting deeper and shallower as seasons change along the path, but the streamline does not get near enough to the surface actually to outcrop until several years before it has arrived at 137°E. In accordance with *Stommel* [1979], we found that outcropping water only leaves the mixed layer in the wintertime.

[18] The age distribution of outcropping layers is summarized in Figure 3, which shows in latitude-density space the age of water on streamlines and the location at which a particular streamline arrives at 137°E. The deeper the isopycnal, the longer the water takes to get to 137°E. The shallowest isopycnal studied shows ages as low as 0.5 years, while for the deepest isopycnal with an outcrop, 26.5 σ_θ , the one streamline whose outcrop could be located takes over 35 years. In the deeper layers the oldest water is to the south. On the 24.5–25.5 isopycnals, water at the southern end of the ventilated area can be 2–3 times older

than water at the northern end. There is also a trend, seen farther up in the water column, of the oldest water being in the middle of this area. This is most visible on the 23, 23.5, 24, and 24.5 isopycnals. There is a hint of a confirmation of this by *Kaneko et al.* [1998], who show a doming of oxygen and nutrient isolines near 17°N in their high-resolution section along 137°–142°E. *Kato* [1998] also shows this feature in an average of sections along 137°E in winter but not in summer. The reason the waters in the middle of this area are older is explained this way. Waters that outcrop near 137°E have a short distance to travel and thus arrive there relatively quickly. Waters that outcrop in the eastern North Pacific have a farther distance to travel but are advected relatively rapidly in the North Equatorial Current. Thus the streamlines that outcrop in the mid-ocean take the longest to get to the observation point. This can be seen in the streamline 5 on 24.0 σ_θ , (Figure 1b), which flows very slowly near its outcrop, and takes a long time, 8.5 years, to reach 137°. The 13.4 year age calculated for a streamline on 23.5 σ_θ takes so long because of very slow flow near its outcrop. This may be too slow, but we believe the tendency to be real.

[19] Ages calculated by this method are similar to those calculated by *Warner et al.* [1996] from *p*CFC-11 measurements, with differences increasing with increasing density [see *Warner et al.*, 1996, Figure 6]. On the 25.4 σ_θ surface,

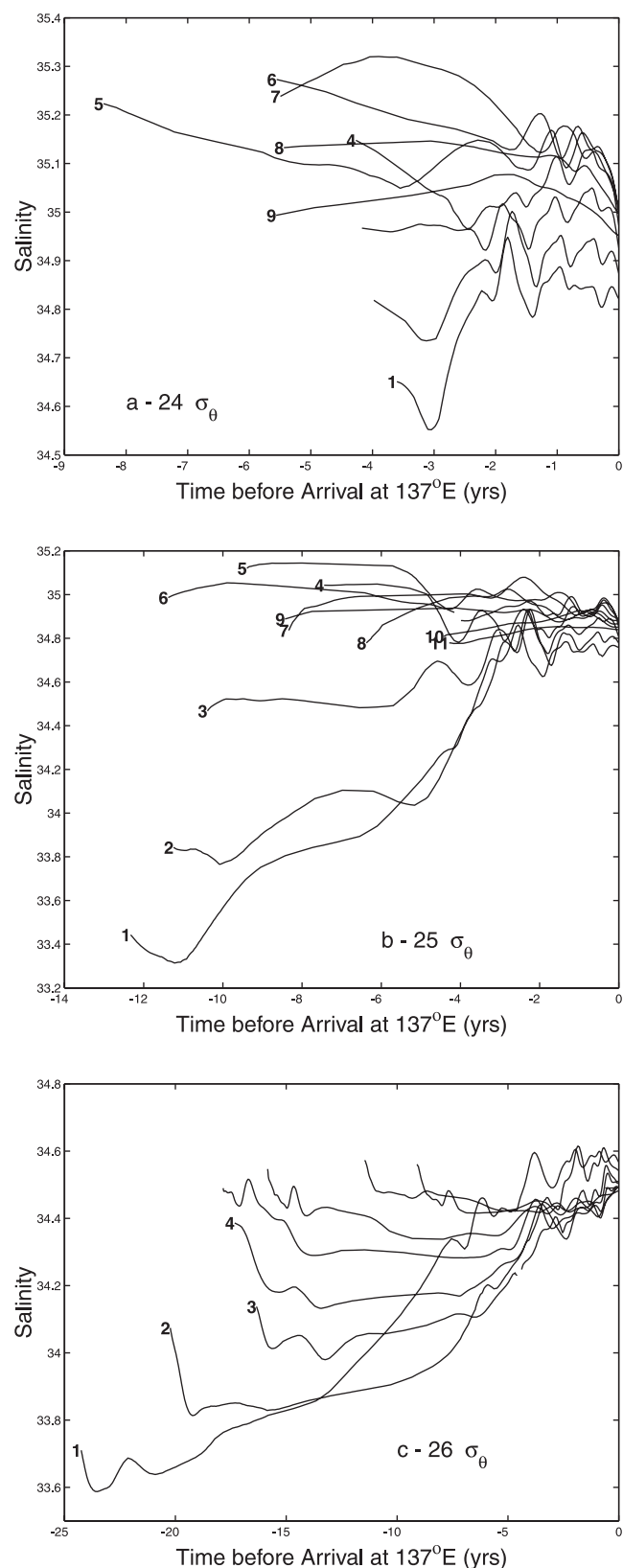


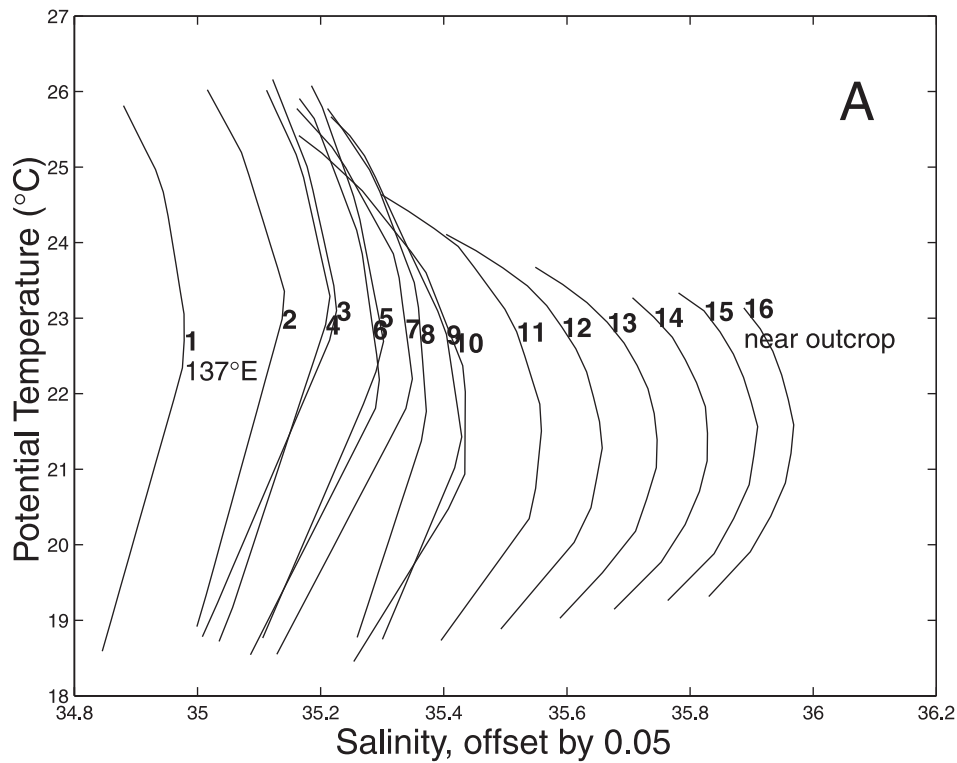
Figure 5. Salinity along streamlines for (a) 24.0, (b) 25.0, and (c) 26.0 σ_θ . Values on the left end of each curve represent the outcrop. Values at the right of each streamline represent the salinity of the streamline when it arrives at 137°E. Numbers on the streamlines correspond to numbers in Figures 1b–1d.

Warner et al. find ages of 8–12 years between 8° and about 18°N. Our method finds ages of 7–15 years on 25.5 σ_θ between 10° and 20°N (Figure 3). On 26.0 σ_θ , north of 8°N, Warner et al. found ages of 16 years or less. Our method finds ages of 16–24 years between 10° and 16°N. At 26.4 σ_θ , Warner et al. found ages of about 20 years along 137°E, while our method finds an age of 35 years at 26.5 σ_θ at 12°N. Warner et al. do note some caveats associated with *p*CFC-11 apparent ages. The ages calculated are biased by mixing between old and young waters, with the bias making older waters seem younger than they actually are. The older the water involved in the mixture, the greater this bias. Also, Warner et al. do not have any CFC measurements between 8° and 24°N along 137°E. The age values quoted above are interpolated using an unstated method. Warner et al. do find the same trend that we do of increasing age on an isopycnal as one goes to the south.

[20] A comparison was done (Figure 4) between the θ -*S* relation at the isopycnal outcrops of the streamlines (asterisks connected with lines) and the 137°E data from the *WOA94* (lines). There is clearly a discrepancy between the outcrop θ -*S* relation and the observed θ -*S* at 137°E. For densities $>\sim 25.0 \sigma_\theta$, the outcrop salinities are mostly lower than the observed. For densities $<25.0 \sigma_\theta$ the outcrop salinities are higher. Also plotted here is the range of θ -*S* values on the outcrop of three isopycnals in March. To obtain these values, we used *WOA94* analyzed values at the surface in March to locate each of the three isopycnals, and then found the range of θ -*S* values along that line. (The asterisks in Figure 4 do not fall exactly along these lines because they are interpolated mixed layer values of θ and *S* for an exact outcrop time and location. The heavy lines are surface values from March.) The lines show the potential range of θ and *S* values available for subduction. The asterisks are the actual values picked out of this range by the reverse trajectory calculation.

[21] The discrepancy between the outcrop θ -*S* relation and that observed at 137°E can be explained by interior along-path changes in salinity as water flows on an isopycnal. By superimposing the flow paths shown in Figure 1 on salinity on the same isopycnals (not shown), one can see that outcrop salinities are very low for the streamlines that outcrop at the eastern side of the basin. These streamlines cross a salinity front soon after subducting in the eastern North Pacific. This front is the boundary between a low-salinity tongue extending westward from the eastern boundary and mid-ocean waters, which are higher salinity. *Suga et al.* [2000; Figure 4] show along-path changes in salinity also occur in waters that outcrop in the surface salinity high in the central subtropical gyre. The salinity of this water decreases along the flow path between the outcrop and the observation point at 137°E. Similar results showing streamlines crossing salinity fronts were shown by *Tsuchiya* [1968, 1982] and *Suga et al.* [2000]. The low-salinity tongue derived from the subarctic frontal zone is explained by a modified *Luyten et al.* [1983] model [*Talley*, 1985]. Since this type of model itself does not reproduce temperature and salinity distributions on isopycnals, it does not explain along-path changes in temperature and salinity in detail. However, our results suggest that the streamlines cross fronts and that mixing must be especially important in this area.

θ - S relation along #4 streamline, $24 \sigma_{\theta}$, 100 day increment



θ - S relation along #6 streamline, $24 \sigma_{\theta}$, 100 day increment

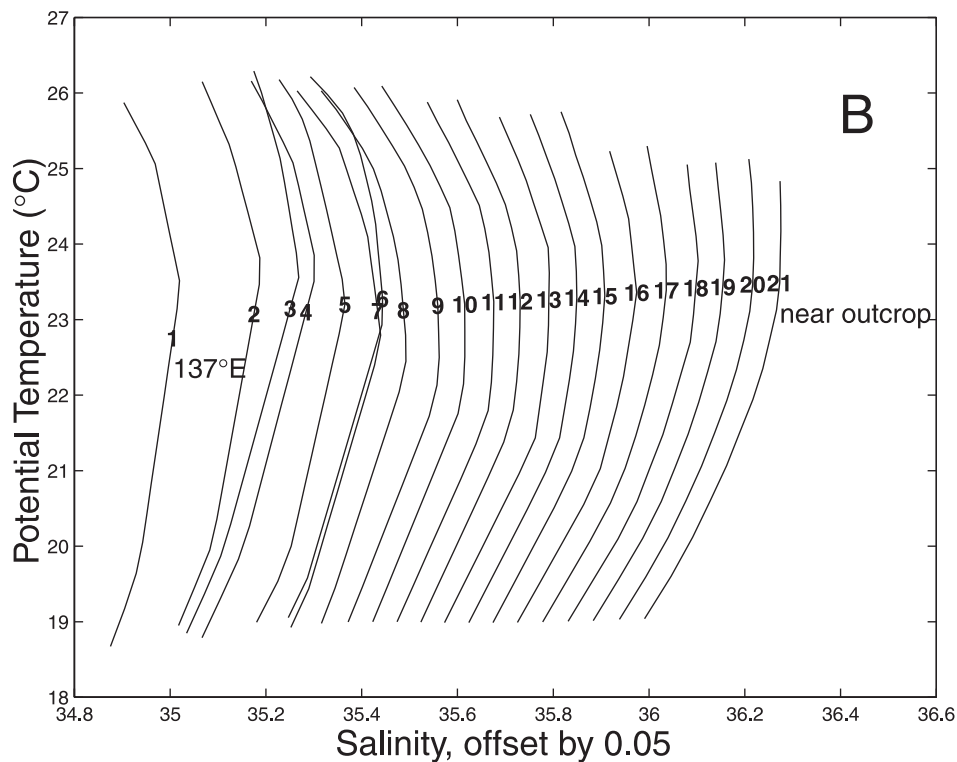


Figure 6. Evolution of θ - S relation along streamlines for $24.0 \sigma_{\theta}$: (a) streamline 4 and (b) streamline 6 (see Figure 1b). The θ - S curves are offset by 0.05. The far left curve is the observed θ - S at 137°E from *WOA94* with no offset. Subsequent curves to the right show the θ - S relation as it goes backward in time to the outcrop. Each curve represents 100 day increments backward in time. The numbers show the actual θ - S value at $24.0 \sigma_{\theta}$.

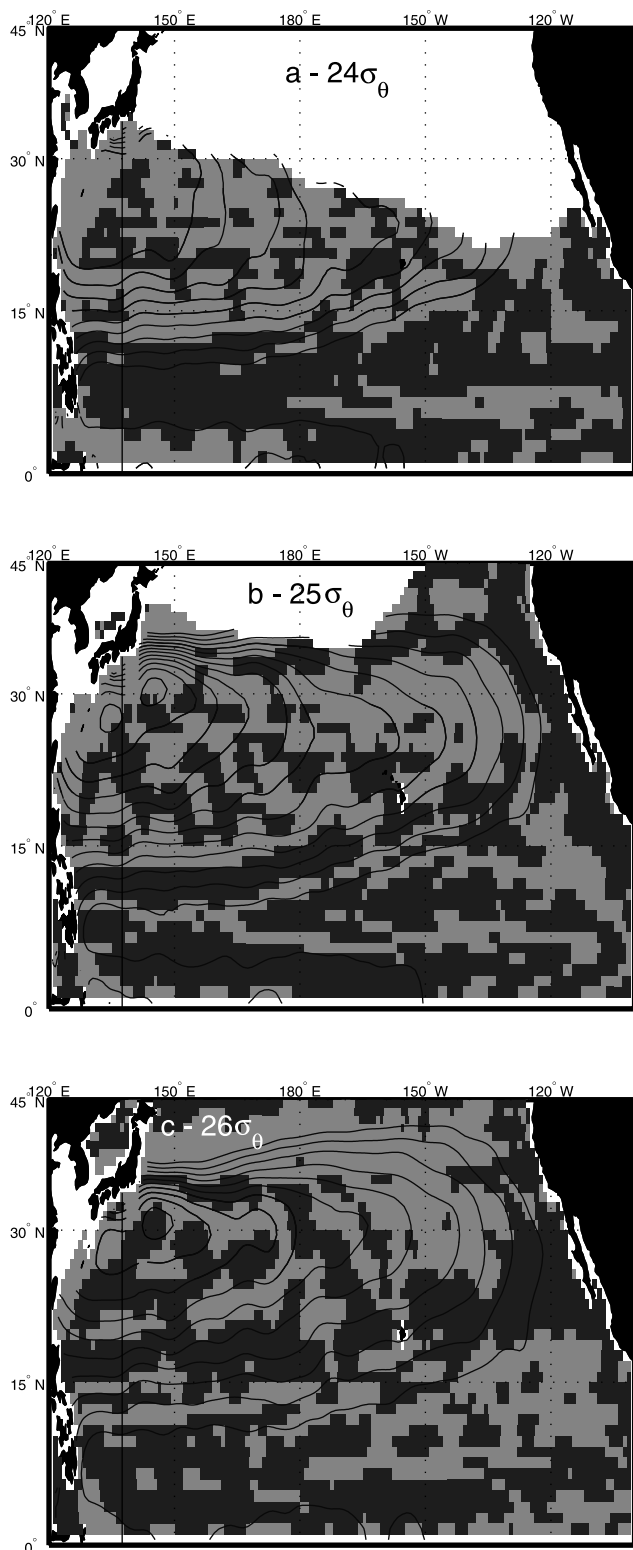
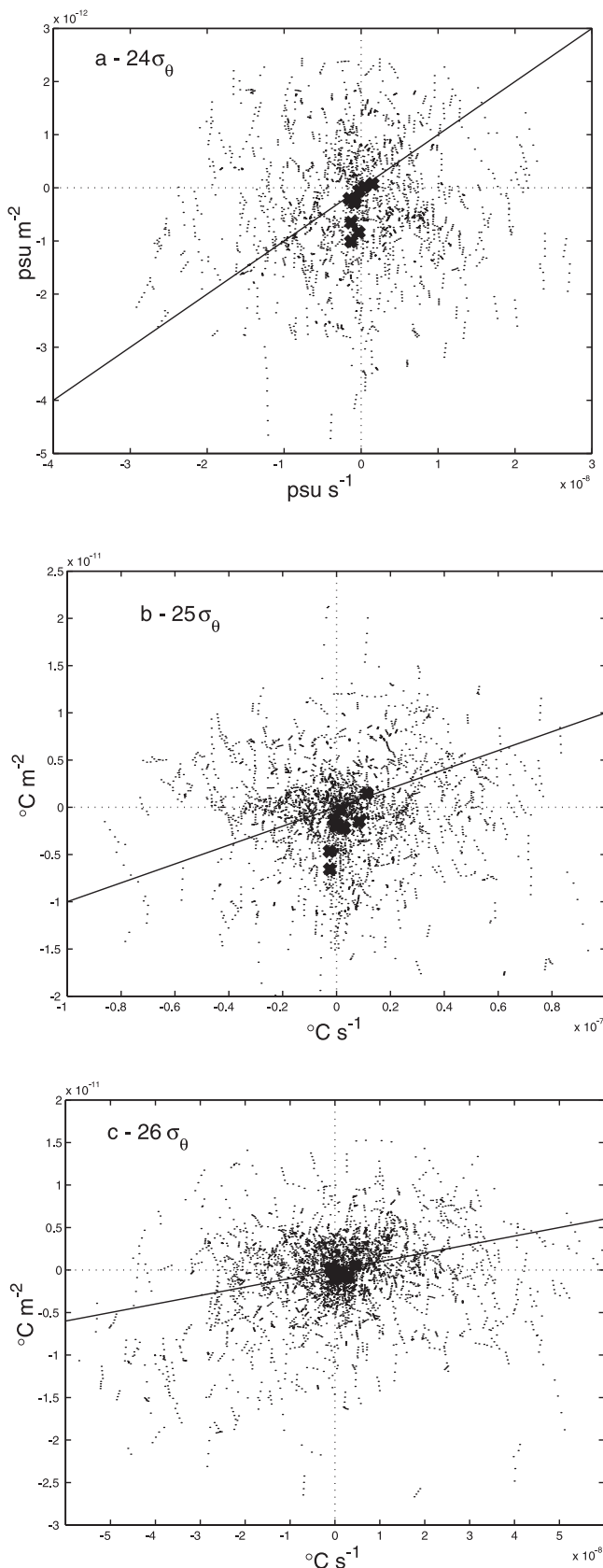


Figure 7. $\nabla^2 S$: (a) 24.0, (b) 25.0, and (c) 26.0 σ_θ . For clarity, instead of contouring the quantity, we shaded positive areas dark and the negative areas light. Superimposed are acceleration potential streamlines from Figure 1b.

[22] In Figures 5a–5c we examine salinity following streamlines on the 24.0, 25.0, and 26.0 σ_θ density surfaces. The right-hand side of each figure marks the point where the water would be observed at 137°E. We work backward in time to the left, plotting the salinity at each point along the flow path with the outcrop points marked with numbers. What is clear for each isopycnal surface is the amount of homogenizing that occurs along flow paths. Starting from a wide range found at the outcrops, the salinities are quite uniform by the time they reach 137°E. For the 24.0 σ_θ surface the total range of salinities at the outcrops is approximately 34.6–35.3, or 0.7. The range observed at 137°E is 34.8–35.0, or a total range of 0.2. This process is even more striking on the 25.0 σ_θ surface. The initial outcrop range is 33.4–35.1, whereas the final range is 34.7–34.9. For some of the streamlines, the salinity increases along the path (e.g., streamline 1 for 24 σ_θ), whereas for some streamlines, it decreases (e.g., streamline 6 for 24.0 σ_θ). The streamlines where the salinity increases along the path mainly outcrop in the eastern North Pacific, and the increase along the path occurs as they cross the salinity front discussed above. The streamlines where an along-path decrease in salinity is seen outcrop in the high surface salinity area of the central North Pacific.

[23] To examine further the along-path changes in salinity, we look in detail at the θ - S relationship as it evolves along two streamlines on the 24.0 σ_θ surface. This surface is approximately the center of the NPTW salinity maximum observed along 137°E. For streamline 4 (Figure 6a) the θ - S curve at 137°E is the one farthest to the left with successive θ - S relations plotted at 100 day intervals going backward along the streamline until the last one before the outcrop is plotted at the right. It should be noted here that the waters above and below the streamline have different trajectories, and waters are not flowing as a column. Streamline 4 outcrops in the eastern North Pacific above the salinity maximum water of the central gyre and stays above it for the most part on its journey to 137°E. It is only when it gets near to 137°E that it ends up being part of the salinity maximum observed there. The other feature to note in this progression is the reduction of curvature of the θ - S relation along the streamline. This is strongly suggestive of diapycnal mixing's being as an important process since it depends on the curvature of the θ - S relation, as will be discussed below. Diapycnal mixing tends to smooth out curvature in the θ - S relation.

[24] The number 6 streamline (Figures 1b and 6b), by contrast, outcrops in the middle of the high-salinity central North Pacific. As it flows along, successively fresher waters appear above it, making it a part of the salinity maximum throughout its path to 137°E. The curvature of the θ - S relation is small compared to the streamline illustrated in Figure 6a, especially before the thousandth day, and appears to increase slightly along the flow path. Compared to the streamline illustrated in Figure 6a, there is relatively little along-path change in salinity (see Figure 5a), suggesting weak mixing. At the very end of its path the salinity decreases quickly as seen by the enhanced spacing between curves 1 and 2. The streamline passes through the end of a tongue of high-salinity water emanating from the central subtropical gyre.



[25] The main candidates for processes that drive the along-streamline changes in salinity are diapycnal and isopycnal mixing. *McDougall* [1984] presents an equation for changes in salinity on a neutral surface [*McDougall*, 1984, last appendix equation]. We rewrite that equation in a Lagrangian framework following *Joyce et al.* [1998]:

$$S_t = \kappa \nabla^2 S + \frac{gD}{N^2} \theta_d^3 \alpha \frac{\partial^2 S}{\partial \theta^2}, \quad (1)$$

where S is the salinity, S_t is the time rate of change of salinity following a water parcel, κ is the isopycnal diffusivity, D is the diapycnal diffusivity, g is the acceleration of gravity, N is the Brunt-Vaisala frequency, σ_d is the gradient of potential temperature across isopycnal surfaces, α is the thermal expansion coefficient, and $\partial^2 S / \partial \theta^2$ is the local curvature of the θ - S relation. We have neglected double-diffusive and nonlinear equation of state terms in equation (1). *Jackett and McDougall* [1997] have shown that neutral surfaces are very close to isopycnals in the shallow North Pacific, so we use isopycnals here. The first term on the right-hand side is isopycnal mixing, and the second term is diapycnal mixing. Note that in the second term the strength of the mixing is proportional to the curvature of the θ - S relation $\partial^2 S / \partial \theta^2$.

[26] The balance in equation (1) can be evaluated to show what values of vertical and horizontal diffusivity are required to account for the observed along-path changes in salinity. The term on the left-hand side of equation (1) can be estimated from Figure 5. We assumed values of κ and D for the right-hand side of equation (1) and estimated the terms from using *WOA94* data to see if they are consistent with the time rate of change in S from the left-hand side of equation (1).

[27] We have calculated $\nabla^2 S$ on the $24.0 \sigma_\theta$ isopycnal over the entire North Pacific. The result of this calculation is somewhat noisy, but we can get a sense of the distribution from Figure 7a. There are coherent areas of positive or negative $\nabla^2 S$. We can see streamlines on $24.0 \sigma_\theta$ that do not unambiguously flow in one regime or another. To elucidate this point further, we show in Figure 8a a scatter of changes in S along streamlines and $\nabla^2 S$. To get this quantity, we interpolated between *WOA94* grid points to each streamline. We note there is no visible correlation between the two. The line in Figure 8a is $\kappa = 1 \times 10^4 \text{ m}^2 \text{ s}^{-1}$, a commonly used value for the horizontal diffusivity [*Hosoda et al.*, 2001]. If eddy diffusion applied exactly, with a constant diffusion coefficient, all the points in the Figure 8a would lie on a straight line something like the line shown. We also calculated along-streamline averages of $\nabla^2 S$ and $\partial S / \partial t$. Average $\partial S / \partial t$ was calculated by simply taking the differ-

Figure 8. (opposite) $\nabla^2 S$ along the streamlines shown in Figure 7 versus $\partial S / \partial t$: (a) 24.0 , (b) 25.0 , and (c) $26.0 \sigma_\theta$. Crossed lines indicate zero of each quantity. Large crosses are streamline averages described in the text. Diagonal lines shows where points should line up for $\kappa = 1 \times 10^4 \text{ m}^2 \text{ s}^{-1}$ according to equation (1) with no diapycnal mixing. Dots are individual estimates of each quantity along the streamlines. Note that Figures 8a–8c each have different axis limits in order to best display the data.

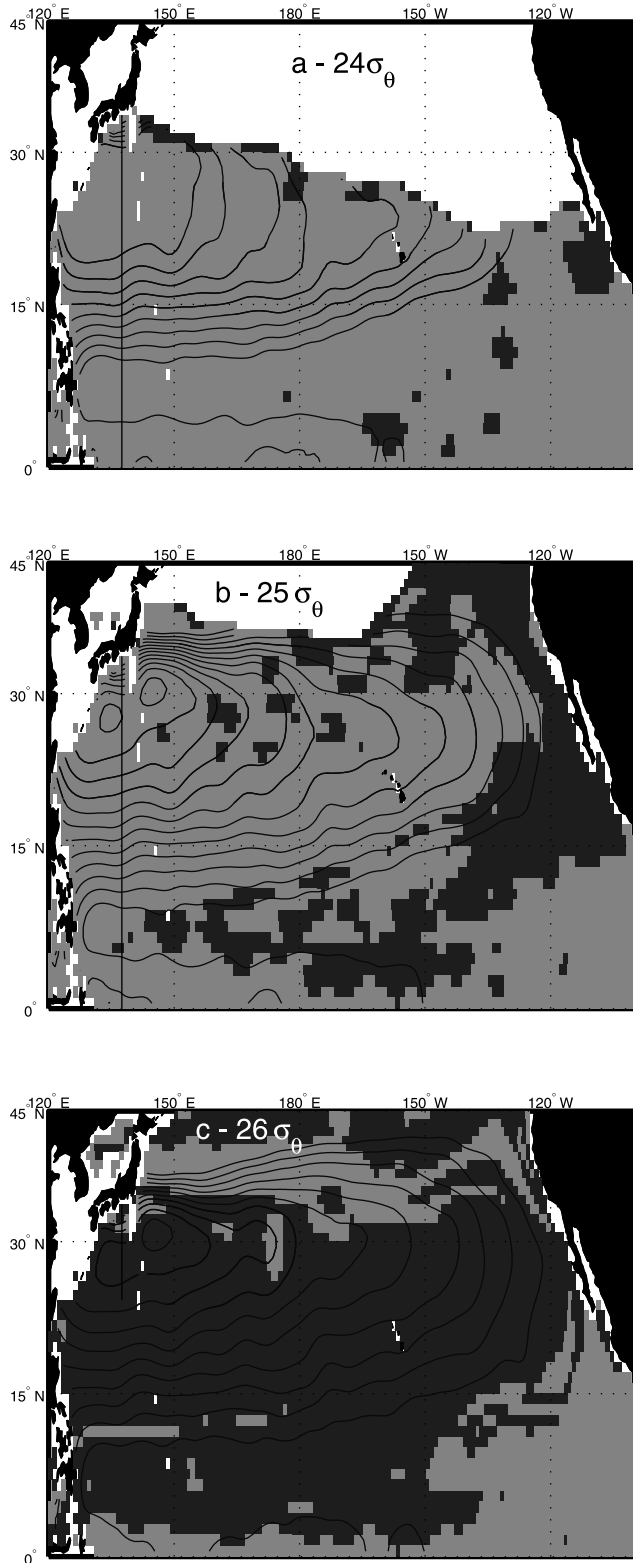


Figure 9. Second term in equation (1) without the diffusion coefficient, $gN^{-2}\theta_d^3\alpha(\partial^2S/\partial\theta^2)$: (a) 24.0, (b) 25.0, and (c) 26.0 σ_θ . For clarity, instead of contouring the quantity we shaded positive areas dark and negative areas light. Superimposed are acceleration potential streamlines from Figure 1b.

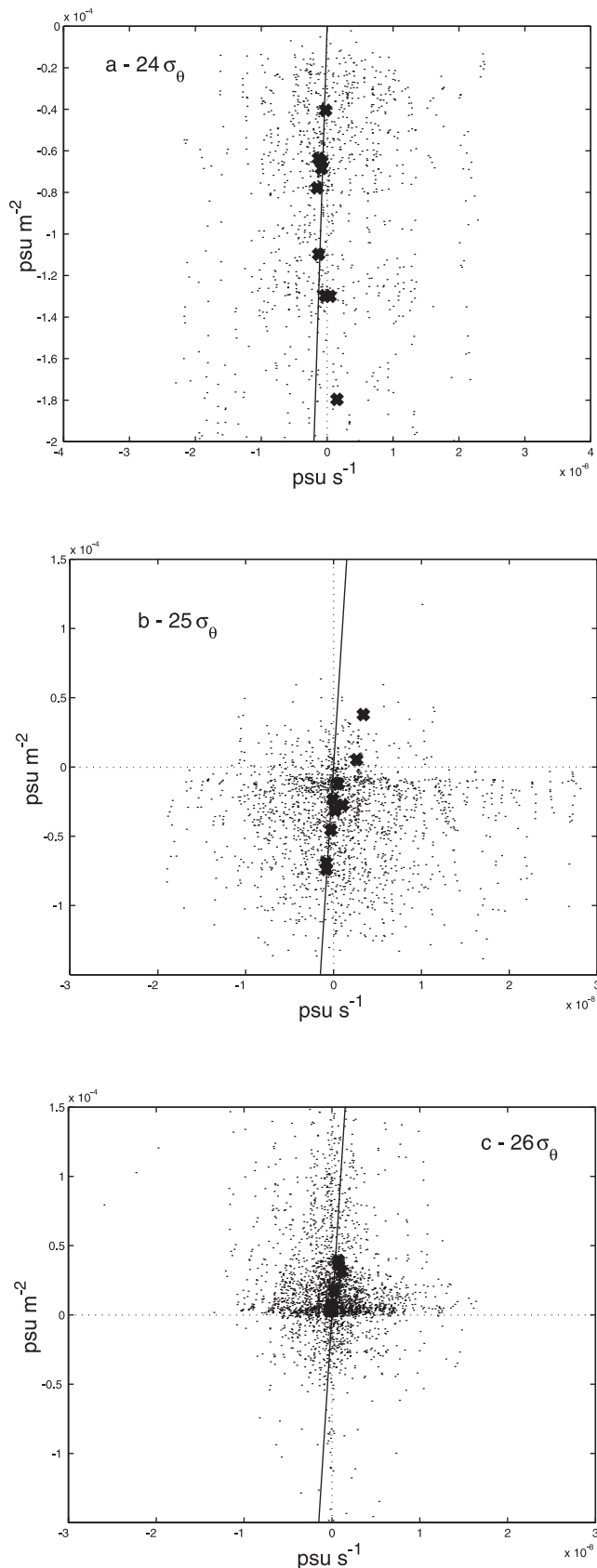
ence between the beginning and ending S (read from Figure 5a) and dividing by the total time taken (abscissa in Figure 5a). The average of ∇^2S was calculated by averaging the quantity along the streamline and weighting individually averaged points by the amount of time spent in a given area. Again, there is no particular correlation between the two quantities.

[28] We estimated the other term on the right-hand side of equation (1) for 24.0 σ_θ over the entire North Pacific, and plotted it in Figure 9a. As one can see, the term is negative nearly everywhere because of the curvature of the θ - S relation at this density level (Figures 6a and 6b). We did a similar scatterplot of the second term of equation (1) (all except D) against the change in S with time (Figure 10a). To do this, we interpolated the field to the spatial locations of the streamlines. As we see, the scatterplot shows all negative values of the term. (A small number of positive values were omitted from the plot.) The line in Figure 10a shows $D = 1 \times 10^{-5} \text{ m}^2 \text{ s}^{-1}$, a typical value cited in the literature [Ledwell *et al.*, 1993]. We see again that the points do not all line up along this line. There is to be more tendency to line up than we saw in Figure 8a, though. This can be seen in the streamline-averaged values shown in Figure 10a. These values appear to line up along the straight line. The best fit slope to these points gives a value of D of $1.51 \times 10^{-5} \text{ m}^2 \text{ s}^{-1}$. The three lowest points are for the first three streamlines, leaving the mixed layer in the far eastern North Pacific. These points do not fall as closely on the straight line drawn. Since they cross a salinity front soon after leaving the outcrop, the mixing process may not be as simple as for the other streamlines.

[29] Calculation of the $S_{\theta\theta}$ term and ∇^2S for the other two surfaces, 25.0 and 26.0 σ_θ (Figures 7–10), highlight our interpretation. On all of the surfaces, ∇^2S is noisy and not consistently of one sign or the other. On the 24 σ_θ surface the $S_{\theta\theta}$ term is mainly negative (light). On the 25.0 σ_θ surface it is mixed, and on the 26.0 surface it is mainly positive (dark). This is a demonstration of the underlying water mass structure in the North Pacific. There is a salinity maximum (NPTW) near 24 σ_θ with the θ - S curvature in one sense and a salinity minimum near 26.8 σ_θ [Talley, 1993] with the θ - S curvature in the other sense. The 26.0 σ_θ surface lies at the top of this feature.

[30] From this analysis it appears that isopycnal diffusivity plays little role in the observed homogenization of water masses observed at 137°E. Large-scale distributions of ∇^2S are not consistently of one sign or the other. Diapycnal diffusivity is somewhat more consistent with the observed changes of potential temperature on this isopycnal, especially when heavily averaged, but clearly is not acting alone, or according to a simple theory. Diapycnal diffusivity will tend to flatten out vertical maxima or minima, as seen in Figure 6a.

[31] Bauer and Siedler [1988] concluded that, for a similar isopycnal in the North Atlantic, double-diffusive processes were dominant. To estimate the importance of double diffusion, we calculated density ratio [Laurent and Schmitt, 1999; Turner, 1973] for three isopycnals, 24.0, 25.0, and 26.0 σ_θ (not shown) using WOA94 data. The density ratio is defined at $R_\rho = \alpha\theta_z(\beta S_z)^{-1}$, where α is the thermal expansion coefficient, β is the saline contraction coefficient, and θ_z and S_z are the vertical gradients of



potential temperature and salinity, respectively. R_ρ indicates the stability of the water column to during double diffusive processes. If the density ratio is >1 , the water column is unstable to salt fingering, but if the ratio is >2 , the instability results in negligible vertical flux of heat or salt. Along most of the isopycnals shown, the density ratio >2 , indicating that double diffusion is not an important process driving the observed homogenization. Our calculation showed a potential area where double diffusion might play an important role near 150°W. Definitive determination of areas of double diffusion await examination of recent high vertical resolution data sets in the Pacific.

[32] The results presented here differ from those of *Robbins et al.* [2000]. Using a one-dimensional stream tube model in the eastern North Atlantic, they found that transient tracer distributions were consistent with strong lateral mixing across property fronts, and that vertical mixing was relatively unimportant. They looked at an equivalent surface in the North Atlantic that was somewhat deeper than the 26.0 σ_θ we examined in the North Pacific. They also found a sharp increase in lateral diffusivity below the base of the thermocline.

4. Discussion

[33] There has been much interest recently in the Pacific shallow overturning circulation [*Talley, 1999*], and plans are being formulated to study it. Our work has several implications for this circulation and our understanding of it. It is clear from the maps of Figure 1 that the interior pathways in the North Pacific are much less important than western boundary pathways for getting water from surface outcropping areas to the tropical current systems [*Johnson and McPhaden, 1999; McCreary and Lu, 1994; Liu et al., 1994*]. That is, water that gets into the North Equatorial Countercurrent, the Equatorial Undercurrent, and into the Indonesian Throughflow from outcropping areas of the North Pacific passes through the western boundary. The window through which these waters pass is part of the 137°E section. Examining Figure 1, streamlines that go through the 137°E section at around 15°N turn equatorward once they reach the western boundary. Water observed on the 137°E section south of about 10°N does not outcrop. Therefore the window through which water passes from the subtropical to the tropical circulation is about 5° wide, between 10° and 15°N. This is the area through which temperature and salinity anomalies must pass if they are to propagate signals from outcrop areas to upwelling zones along the equator as part of the subtropical

Figure 10. (opposite) Second term in equation (1) without the diffusion coefficient, $gN^{-2}\theta_0^3\alpha(\partial^2S/\partial\theta^2)$ along streamlines shown in Figure 9 versus $\partial S/\partial t$: (a) 24.0, (b) 25.0, and (c) 26.0 σ_θ . Large dots are streamline averages described in the text. Straight line shows where points should line up for $D = 1 \times 10^{-5} \text{ m}^2 \text{ s}^{-1}$ according to equation (1) with no isopycnal mixing. Dots are individual estimates of each quantity along the streamlines. Note that Figures 10a–10c each have different axis limits in order to display best the data.

cell [Gu and Philander, 1997]. In other words, changes in the strength of the subtropical cell will be affected by changes in the transport of temperature and salt through this window, either by changes in the size of the window, by changes in the flow field, or through temperature and salinity anomalies that may pass through it.

[34] From the maps of Figure 1 it appears that the window just discussed has a direct connection with the surface in the eastern North Pacific. However, the analysis presented in Figures 5a–5c suggests that even though streamlines have very specific outcrop areas, by the time they get far downstream at 137°E, isopycnals are largely homogenized. Properties imprinted on subducted waters are greatly changed by the time they are observed in the ocean interior. There is very little θ - S variation on isopycnals at 137°E compared to that at the outcrop areas (Figure 4). The homogenization is especially strong for streamlines that outcrop in the eastern North Pacific, the ones that are most relevant to the subtropical cell (1 in Figure 5a and 1 and 2 in Figures 5b and 5c) since the path they take is at the southern edge of the gyre and they are most likely to pass through the window into the tropical circulation. The observed homogenization in salinity values on isopycnals suggests that salinity observed at 137°E is strongly, perhaps principally, influenced by interior processes that occur after the water has been subducted. Variability in water characteristics observed at 137°E will show little or no “teleconnection” to precise origination areas at the surface. Kessler [1999] came to a similar conclusion regarding the high-salinity tongue along 165°E in the eastern South Pacific. Rather, such variability will be associated with surface variability integrated over vast areas of the subtropical gyre and with changes in whatever interior mixing is responsible for the observed homogenization.

[35] Consider a water parcel observed at 137°E. Mixing was shown to be important in setting the properties of that parcel. By the time it reaches 137°E it will have mixed with waters either from above and below, or on the same isopycnal. No matter what type of mixing occurs, it is certain it will have substantially mixed with water of some very different age by the time it reaches the observation point. The mixing may also occur with other water parcels that outcropped at very different locations. So what happens to anomalies of spiciness imposed on water parcels at the surface? The picture here is that those anomalies will not simply propagate directly to 137°E but will spread and mix in complicated ways.

[36] Our conclusion about the relative ineffectiveness of isopycnal mixing can be questioned because we use smoothed climatological data that are already homogenized and does not contain strong isopycnal gradients upon which isopycnal mixing can act. The analysis presented here does underestimate isopycnal mixing somewhat because of this problem, but our field still has significant variance of T/S properties at the outcrop. We have shown that isopycnal mixing alone cannot eliminate gradients in the mean T/S properties injected at the mixed layer base in the absence of significant mean isopycnal gradients downstream from the outcrop. Large-scale changes cannot be maintained by the observed time-mean isopycnal gradients. Thus diapycnal mixing must play an important if not crucial role.

[37] There has been recent speculation about air-sea connections between the tropics and subtropics. The mechanism suggested is as follows. Anomalies of heat are input at the surface in the subtropical gyre. Those anomalies are carried to the equator by the subtropical cell and come up to the surface in the eastern Pacific along the equator. They then influence the atmosphere, which carries the anomalies back to the subtropics [Gu and Philander, 1997; Nonaka and Xie, 2000]. Schneider [1999] suggests a similar mechanism, but the anomalies are of spiciness, and they are generated after water has been subducted and associated with anomalous advection. From our view the most direct way that the subtropical atmosphere can influence the subtropical cell in the North Pacific is not by forcing anomalous values of temperature or salt at the surface, but by changing the size and transport through the window discussed above [Suga et al., 2000; Shuto, 1996]. The size of this window is a function of the bifurcation latitude [Qiu and Lukas, 1996], which is in turn a function of the basin-wide distribution of wind stress curl. How and whether the size of the window can be influenced by air-sea interaction along the equator is a subject we are not able to speculate about.

[38] **Acknowledgments.** Financial support was provided by the National Science Foundation under grant OCE-9711300, the Japan Society for the Promotion of Science under its Short-term Invitation Fellowship Program and its Grant-in-aid for Scientific Research (B) 13440138, and the UNCW Center for Marine Science. CMS Contribution 258. WOCE contribution 616. J. Toole (JGR editor) and two anonymous reviewers read our manuscript carefully and provided thoughtful comments.

References

- Bauer, E., and G. Siedler, The relative contributions of isopycnal and diapycnal mixing below the subtropical salinity maximum, *Deep Sea Res., Part A*, 35, 811–837, 1988.
- Boyer, T. P., and S. Levitus, Quality control and processing of historical oceanographic temperature, salinity, and oxygen data, *NOAA Tech. Rep. NESDIS 81*, 64 pp., Natl. Oceanic and Atmos. Admin., Silver Spring, Md., 1994.
- Conkright, M., et al., *World Ocean Database 1998 Data Set Documentation Version 2.0* [CD-ROM], *NOAA Atlas NESDIS 18*, 114 pp., Natl. Oceanic and Atmos. Admin., Silver Spring, Md., 1999.
- Cushman-Roisin, B., Subduction, in *Dynamics of the Oceanic Surface Mixed Layer*, *Hawaii Inst. Geophys. Spec. Publ.*, edited by P. Muller and D. Henderson, pp. 181–196, Hawaii Inst. of Geophys., Honolulu, 1987.
- Deser, C., M. A. Alexander, and M. S. Timlin, Upper-ocean thermal variations in the North Pacific during 1970–1991, *J. Clim.*, 9, 1840–1855, 1996.
- Gu, D., and S. G. H. Philander, Interdecadal climate fluctuations that depend on exchange between the tropics and extratropics, *Science*, 275, 805–807, 1997.
- Hosoda, S., S. P. Xie, K. Takeuchi, and M. Nonaka, Eastern North Pacific Subtropical Mode Water in a GCM: Formation mechanism and salinity effects, *J. Geophys. Res.*, 106, 19,671–19,681, 2001.
- Huang, R., and B. Qiu, Three-dimensional structure of the wind-driven circulation in the subtropical North Pacific, *J. Phys. Oceanogr.*, 24, 1608–1622, 1994.
- Hurlburt, H. E., and E. J. Metzger, Bifurcation of the Kuroshio Extension at the Shatsky Rise, *J. Geophys. Res.*, 103, 7549–7566, 1998.
- Jackett, D. R., and T. J. McDougall, A neutral density variable for the world's oceans, *J. Phys. Oceanogr.*, 27, 237–263, 1997.
- Johnson, G. C., and M. J. McPhaden, Interior pycnocline flow from the subtropical to the equatorial Pacific Ocean, *J. Phys. Oceanogr.*, 29, 3073–3089, 1999.
- Joyce, T. M., J. R. Luyten, A. Kubryakov, F. B. Bahr, and J. S. Pallant, Meso- to large-scale structure of subducting water in the subtropical gyre of the eastern North Atlantic Ocean, *J. Phys. Oceanogr.*, 28, 40–41, 1998.
- Kaneko, I., Y. Takatsuki, H. Kamiya, and S. Kawae, Water property distributions along the WHP-P9 section (137°–142°E) in the western North Pacific, *J. Geophys. Res.*, 103, 12,959–12,984, 1998.

- Karl, D., and R. Lukas, The Hawaii Ocean Time-series (HOT) program: Background, rationale and field implementation, *Deep Sea Res., Part II*, 43, 129–156, 1996.
- Kato, A., Decadal scale variations of surface and intermediate water masses in the subtropical and tropical western North Pacific (in Japanese), M. S. thesis, Grad. School of Sci., Tohoku Univ., Sendai, Jpn., 1998.
- Kessler, W. S., Interannual variability of the subsurface high salinity tongue south of the equator at 165 degree E, *J. Phys. Oceanogr.*, 29, 2038–2049, 1999.
- Laurent, L. S., and R. W. Schmitt, The contribution of salt fingers to vertical mixing in the North Atlantic Tracer Release Experiment, *J. Phys. Oceanogr.*, 29, 1404–1424, 1999.
- Ledwell, J. R., A. J. Watson, and C. D. Law, Evidence for slow mixing across the pycnocline from an open-ocean tracer-release experiment, *Nature*, 34, 701–703, 1993.
- Levitus, S., Climatological atlas of the world ocean, *NOAA Prof. Pap.* 13, 173 pp., U. S. Govt. Print. Off., Washington, D. C., 1982.
- Levitus, S., and T. P. Boyer, *World Ocean Atlas 1994*, vol. 4, *Temperature*, *NOAA Atlas NESDIS*, vol. 4, 129 pp., Natl. Oceanic and Atmos. Admin., Silver Spring, Md., 1994.
- Levitus, S., J. Antonov, and T. Boyer, Interannual variability of temperature at a depth of 125 meters in the North Atlantic Ocean, *Science*, 266, 96–99, 1994a.
- Levitus, S., R. Burgett, and T. P. Boyer, *World Ocean Atlas 1994*, vol. 3, *Salinity*, *NOAA Atlas NESDIS*, vol. 3, 111 pp., Natl. Oceanic and Atmos. Admin., Silver Spring, Md., 1994b.
- Levitus, S., T. Boyer, M. Conkright, T. O'Brien, J. Antonov, C. Stephens, L. Stathopoulos, D. Johnson, and R. Gelfeld, *World Ocean Database 1998*, vol. 1, *Introduction*, *NOAA Atlas NESDIS 18*, 346 pp., Natl. Oceanic and Atmos. Admin., Silver Spring, Md., 1998.
- Liu, Z., S. G. H. Philander, and R. C. Pacanowski, A GCM study of tropical-subtropical upper-ocean water exchange, *J. Phys. Oceanogr.*, 24, 2606–2623, 1994.
- Luyten, J. R., J. Pedlosky, and H. Stommel, The ventilated thermocline, *J. Phys. Oceanogr.*, 13, 292–309, 1983.
- Macdonald, A. M., T. Suga, and R. G. Curry, An isopycnally averaged North Pacific climatology, *J. Atmos. Oceanic Technol.*, 18, 394–420, 2001.
- Marshall, J. C., A. J. G. Nurser, and R. G. Williams, Inferring the subduction rate and period over the North Atlantic, *J. Phys. Oceanogr.*, 23, 1315–1329, 1993.
- McCreary, J., and P. Lu, On the interaction between the subtropical and equatorial ocean circulations: The subtropical cell, *J. Phys. Oceanogr.*, 24, 466–497, 1994.
- McDougall, T. J., The relative roles of diapycnal and isopycnal mixing on subsurface water mass conversion, *J. Phys. Oceanogr.*, 14, 1577–1589, 1984.
- Michaels, A. F., and A. H. Knap, Overview of the U.S. JGOFS Bermuda Atlantic Time-series Study and the Hydrostation S Program, *Deep Sea Res., Part II*, 43, 157–198, 1996.
- Mizuno, K., and W. B. White, Annual and interannual variability in the Kuroshio System, *J. Phys. Oceanogr.*, 13, 1848–1867, 1983.
- Montgomery, R., and E. Stroup, Equatorial waters and currents at 150°W in July–August 1952, *Johns Hopkins Oceanogr. Stud.*, 1, 68 pp., 1962.
- Nonaka, M., and S. P. Xie, Propagation of North Pacific interdecadal subsurface temperature anomalies in an ocean GCM, *Geophys. Res. Lett.*, 27, 3747–3750, 2000.
- Qiu, B., and R. Huang, Ventilation of the North Atlantic and North Pacific: Subduction versus obduction, *J. Phys. Oceanogr.*, 25, 2374–2390, 1995.
- Qiu, B., and R. Lukas, Seasonal and interannual variability of the North Equatorial Current, the Mindanao Current, and the Kuroshio along the Pacific western boundary, *J. Geophys. Res.*, 101, 12,315–12,330, 1996.
- Reid, J., Intermediate waters of the Pacific Ocean, *Johns Hopkins Oceanogr. Stud.*, 2, 85 pp., 1965.
- Robbins, P. E., J. F. Price, W. B. Owens, and W. J. Jenkins, The importance of lateral diffusion for the ventilation of the lower thermocline in the subtropical North Atlantic, *J. Phys. Oceanogr.*, 30, 67–89, 2000.
- Roemmich, D., and B. Cornuelle, The Subtropical Mode Waters of the South Pacific Ocean, *J. Phys. Oceanogr.*, 22, 1178–1187, 1992.
- Roemmich, D., and T. McCallister, Large scale circulation of the North Pacific Ocean, *Prog. Oceanogr.*, 22, 171–204, 1989.
- Roemmich, D., J. Sprintall, S. Yaeger, B. Cornuelle, and R. Bailey, Repeat XBT/XCTD sections in the Pacific, *GCOS Rep. 41*, 7 pp., U.N. Educ., Sci., and Cult. Org., Paris, 1997.
- Schneider, N., A decadal spiciness mode in the tropics, *Geophys. Res. Lett.*, 27, 257–260, 1999.
- Semtner, A., and R. Chervin, A simulation of the global ocean circulation with resolved eddies, *J. Geophys. Res.*, 93, 15,502–15,522, 1988.
- Shuto, K., Interannual variations of water temperature and salinity along the 137°E meridian, *J. Oceanogr.*, 52, 575–595, 1996.
- Sprintall, J., A. Althaus, D. Roemmich, L. Lehmann, B. Cornuelle, and R. Bailey, *High resolution XBT sections in the Pacific and Indian Oceans, 1991–95*, 143 pp., Scripps Inst. of Oceanogr., San Diego, Calif., 1997.
- Stommel, H., Determination of water mass properties of water pumped down from the Ekman layer to the geostrophic flow below, *Proc. Natl. Acad. Sci.*, 76, 3051–3055, 1979.
- Suga, T., and K. Hanawa, Interannual variations of North Pacific Subtropical Mode Water in the 137°E section, *J. Phys. Oceanogr.*, 25, 1012–1017, 1995.
- Suga, T., A. Kato, and K. Hanawa, North Pacific Tropical Water: Its climatology and temporal changes associated with the climate regime shift in the 1970's, *Prog. Oceanogr.*, 47, 223–256, 2000.
- Tabata, S., and W. Weichselbaumer, An update of the statistics of hydrographic/CTD data taken at Ocean Station P (May 1956–September 1990), 83 pp., *Can. Data Rep. Hydrogr. Ocean Sci.*, 107, Inst. of Ocean Sci., Sidney, B. C., 1992.
- Talley, L. D., Ventilation of the subtropical North Pacific: The shallow salinity minimum, *J. Phys. Oceanogr.*, 15, 633–649, 1985.
- Talley, L., Distribution and formation of North Pacific Intermediate Water, *J. Phys. Oceanogr.*, 23, 517–537, 1993.
- Talley, L. D., Some aspects of ocean heat transport by the shallow, intermediate and deep overturning circulations, in *Mechanisms of Global Climate Change at Millennial Time Scales*, *Geophys. Monogr. Ser.*, vol. 112, edited by P. U. Clark, R. S. Webb, and L. D. Keigwin, pp. 1–22, AGU, Washington, D. C., 1999.
- Tanimoto, Y., N. Iwasaka, K. Hanawa, and Y. Toba, Characteristic variations of sea surface temperature with multiple time scales in the North Pacific, *J. Clim.*, 6, 1153–1160, 1993.
- Tsuchiya, M., Upper waters of the intertropical Pacific Ocean, *Johns Hopkins Oceanogr. Stud.*, 4, 50 pp., 1968.
- Tsuchiya, M., On the Pacific upper-water circulation, *J. Mar. Res.*, 40, suppl., 777–799, 1982.
- Turner, J. S., *Buoyancy Effects in Fluids*, 367 pp., Cambridge Univ. Press, New York, 1973.
- Warner, M. J., J. L. Bullister, D. P. Wisegarver, R. H. Gammon, and R. F. Weiss, Basin-wide distributions of chlorofluorocarbons CFC-11 and CFC-12 in the North Pacific: 1985–1989, *J. Geophys. Res.*, 101, 20,525–20,542, 1996.
- Williams, R. G., M. A. Spall, and J. C. Marshall, Does Stommel's mixed layer "demon" work?, *J. Phys. Oceanogr.*, 25, 3089–3102, 1995.
- Woods, J. D., The physics of pycnocline ventilation, in *Coupled Ocean-Atmosphere Models*, edited by J. C. J. Nihoul, pp. 543–590, Elsevier Sci., New York, 1985.
- Yasuda, T., and K. Hanawa, Decadal changes in the mode waters in the midlatitude North Pacific, *J. Phys. Oceanogr.*, 27, 858–870, 1997.

F. M. Bingham, Center for Marine Science, University of North Carolina at Wilmington, Wilmington, NC 28409, USA. (bigkahuna@fredbingham.com)

T. Suga and K. Hanawa, Department of Geophysics, Graduate School of Science, Tohoku University, Sendai, 980-8578, Japan.